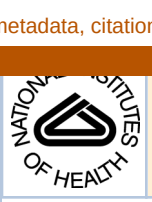

Published in final edited form as:

Arthritis Rheum. 2009 August ; 60(8): 2314–2324. doi:10.1002/art.24704.

Abrogation of Antibody-Induced Arthritis in Mice by a Self-Activating Viridin Prodrug and Association With Impaired Neutrophil and Endothelial Cell Function

Lars Stangenberg, MD[1], **Chris Ellson, PhD**[2], **Virna Cortez-Retamozo, PhD**[1], **Adriana Ortiz-Lopez, PhD**[3], **Hushan Yuan, PhD**[1], **Joseph Blois, PhD**[1], **Ralph A. Smith, PhD**[1], **Michael B. Yaffe, MD, PhD**[2], **Ralph Weissleder, MD, PhD**[1], **Christophe Benoist, MD, PhD**[3], **Diane Mathis, PhD**[3], **Lee Josephson, PhD**[1], and **Umar Mahmood, MD PhD**[1]

[1]Massachusetts General Hospital, and Harvard Medical School, Boston, Massachusetts

[2]Massachusetts Institute of Technology, Cambridge

[3]Harvard Medical School, Boston, and Broad Institute of Harvard and MIT, Cambridge, Massachusetts.

Abstract

Objective—To test a novel self-activating viridin (SAV) prodrug that slowly releases wortmannin, a potent phosphoinositide 3-kinase inhibitor, in a model of antibody-mediated inflammatory arthritis.

Methods—The SAV prodrug was administered to K/BxN mice or to C57BL/6 (B6) mice that had been injected with K/BxN serum. Ankle thickness was measured, and histologic changes were scored after a 10-day disease course (serum-transfer arthritis). Protease activity was measured by a near-infrared imaging approach using a cleavable cathepsin–selective probe. Further near-infrared imaging techniques were used to analyze early changes in vascular permeability after serum injection, as well as neutrophil–endothelial cell interactions. Neutrophil functions were assessed using an oxidative burst assay as well as a degranulation assay.

Results—SAV prevented ankle swelling in mice with serum-transfer arthritis in a dose-dependent manner. It also markedly reduced the extent of other features of arthritis, such as protease activity and histology scores for inflammation and joint erosion. Moreover, SAV was an effective therapeutic agent. The underlying mechanisms for the antiinflammatory activity were

Address correspondence and reprint requests to Umar Mahmood, MD, PhD, Nuclear Medicine and Molecular Imaging, Department of Radiology, Massachusetts General Hospital, 55 Fruit Street, White 427, Boston, MA 02114. umahmood@mgh.harvard.edu.

AUTHOR CONTRIBUTIONS

All authors were involved in drafting the article or revising it critically for important intellectual content, and all authors approved the final version to be published. Dr. Mahmood had full access to all of the data in the study and takes responsibility for the integrity of the data and the accuracy of the data analysis.

Study conception and design. Stangenberg, Yuan, Blois, Smith, Weissleder, Benoist, Mathis, Josephson, Mahmood.

Acquisition of data. Stangenberg, Ellson, Cortez-Retamozo, Ortiz- Lopez, Weissleder.

Analysis and interpretation of data. Stangenberg, Ellson, Cortez-Retamozo, Yaffe, Weissleder, Benoist, Mathis, Josephson, Mahmood.

Synthesis and characterization of compound. Yuan, Blois, Smith.

Dr. Weissleder owns stock in VisEn Medical and has served as a paid consultant with investment analysts on behalf of T2 Biosystems. Dr. Mahmood has received consulting fees from VisEn Medical (less than $10,000). Drs. Weissleder, Josephson, and Mahmood (along with other Massachusetts General Hospital [MGH] employees) are coinventors on a patent owned by MGH for intramolecularly quenched near-infrared fluorescent probes; VisEn Medical has licensed the patent, and the authors therefore receive (minimal) royalties.

manifold. Endothelial permeability after serum injection was reduced, as was firm neutrophil attachment to endothelial cells. Endothelial cell activation by tumor necrosis factor α was impeded by SAV, as measured by the expression of vascular cell adhesion molecule. Crucial neutrophil functions, such as generation of reactive oxygen species and degranulation of protease-laden vesicles, were decreased by SAV administration.

Conclusion—A novel SAV prodrug proved strongly antiinflammatory in a murine model of antibody-induced inflammatory arthritis. Its activity could be attributed, at least in part, to the inhibition of neutrophil and endothelial cell functions.

Rheumatoid arthritis (RA) is a complex disease that involves multiple cell types in its initiation and maintenance. Cells of the adaptive immune system are involved at the beginning, as activated T cells initiate a cytokine cascade that subsequently stimulates effector cells. T cells are also important in promoting a humoral immune response, inducing B cell proliferation as well as antibody production and class switching. Later stages of the disease are dependent on cells of the innate immune system. These activated effector cells, such as monocyte/macrophages and neutrophils, establish and entertain a proinflammatory cytokine network. The importance of this proinflammatory cytokine network in RA was recently highlighted by the clinical success of new therapeutic drugs that target the interleukin-1 (IL-1) receptor (1,2) and tumor necrosis factor α (TNFα) (3–6). Effector cells also release proteolytic enzymes that destroy the bone and cartilage structures of the joints, culminating in the symptoms of RA.

All of these immune cells rely on extracellular and intracellular signaling to function properly. Kinases are crucial parts of this signaling network, since they link both compartments and provide amplification. In particular, phosphatidylinositol 3-kinases (PI3Ks) are required for full functionality, as has clearly been demonstrated in mouse models. Mice without PI3Kγ signaling exhibited impaired neutrophil functions, in particular migration and oxidative burst, after stimulation (7–9). Likewise, the migration of macrophages was diminished (7). There was incomplete T cell activation, leading to reduced proliferation and cytokine production after stimulation (8,9). In contrast, PI3Kδ-knockout mice showed impaired B cell functionality, with reduced numbers of B cells, diminished levels of serum immunoglobulins, impaired proliferative capacity, and a higher rate of apoptosis (10,11). Mast cell–driven conditions, such as allergic responses and passive anaphylaxis, were found to be impaired in both PI3Kγ-deficient and PI3Kδ-deficient mice (12,13). PI3Kγ-deficient and PI3Kδ-deficient mice were also found to be partly protected from inflammatory arthritis in several models: collagen-induced arthritis, collagen antibody–induced arthritis, K/BxN serum–transfer arthritis (14,15). Most strikingly, a double-knockout mouse for both isoforms was shown to be completely protected from inflammation, edema formation, and destruction of articular structures (15), suggesting that inhibitors of multiple PI3K isotypes might also have particular therapeutic potential.

The viridin wortmannin is a highly potent, but nonselective, inhibitor of PI3K isoforms, with a 50% inhibition concentration of ~5 n*M* (16,17). It is a fungal metabolite and structurally resembles a steroid with an additional furan ring. Wortmannin irreversibly inhibits PI3Ks by a covalent reaction with a lysine residue in the ATP-binding pocket of the catalytic subunit (18,19). Long before PI3Ks were identified as primary targets of wortmannin, its antiinflammatory properties were described (20), and it has often been used in the study of PI3K signaling (21).

Recently, we reported that under physiologic conditions, wortmannin reacts reversibly with certain nucleophiles at the C20 position (22) and used this observation to design the self-activating viridin (SAV) prodrug shown in Figure 1. SAV is an inactive prodrug. It does not inhibit PI3K, but slowly releases active wortmannin, with a half-time of 9 hours. SAV uses a

dextran carrier to improve solubility in aqueous solutions, increase circulation time, and decrease the membrane permeability of its attached wortmannin. Once released, however, wortmannin is membrane-permeable and can thus exert its effects on intracellular target kinases. Despite its modification at the C20 position, SAV is a more potent compound than wortmannin when evaluated in long-term cell-based antiproliferative assays (rather than short-term PI3K assays), as one would expect due to its slow release of active wortmannin and consequent long duration of action (23).

In the present study, we tested the activity of SAV in the K/BxN mouse model of antibody-induced inflammatory arthritis. We hypothesized that due to its nonisotype selective inhibition of PI3Ks, SAV might exert antiinflammatory activity in this model, and upon finding that this was indeed the case, we investigated the underlying cellular mechanisms that contributed to that activity.

MATERIALS AND METHODS

Synthesis of SAV

SAV and carrier control were synthesized in a custom-made manner. A detailed description of the synthesis has been published elsewhere (23).

Mice

B6 mice ages 6–8 weeks were purchased from The Jackson Laboratory (Bar Harbor, ME). KRN T cell receptor–transgenic mice were maintained on the B6 genetic background (K/B6). Crossing K/B6 animals with NOD mice generated arthritic K/BxN offspring, as described previously (24). All mouse procedures were approved by the Institutional Subcommittee on Research Animal Care at Massachusetts General Hospital.

Arthritis models and treatments

K/BxN mice developed arthritis between 25 and 35 days of age. In the prevention setting, SAV was administered intraperitoneally (IP) to K/BxN mice beginning on day 23 of age. The dose was equivalent to 0.75 mg of wortmannin/kg of body weight. Injections were repeated daily for 25 days.

Serum-transfer arthritis was induced in B6 mice by IP injection of 150 μl of pooled serum from 8-week-old K/BxN mice on days 0 and 2. Prevention studies were performed in B6 mice by beginning treatment on day 0 and ending on day 10. For the prevention studies, IP injections of SAV were administered daily to 3 groups of mice at 1 of 3 dosages of 0.75 mg/kg, 0.25 mg/kg, or 0.083 mg/kg. Intervention studies were performed in B6 mice by beginning treatment on day 6 and ending on day 10. For the intervention studies, SAV was administered IP at a dosage of 0.75 mg/kg.

In K/BxN mice and B6 mice, carrier control was injected at a dosage of 0.75 mg/kg. Clinical arthritis was assessed by measuring ankle thickness.

Histologic analysis

Paws were fixed in 10% formalin and decalcified in 0.2*M* EDTA over 3 days. Specimens were paraffin-embedded, and sections were cut in the sagittal plane. Standard hematoxylin and eosin staining was used to assess arthritic joints. Inflammation and cartilage destruction were evaluated and scored (14). Inflammation was scored on a scale of 0–4, where 0 = no inflammation, 1 = slight thickening of the lining layer or some infiltrating cells in the sublining layer, 2 = slight thickening of the lining layer plus some infiltrating cells in the sublining layer, 3 = thickening of the lining layer, influx of cells in the sublining layer, and

the presence of cells in the synovial space, and 4 = synovium highly infiltrated with many inflammatory cells. Cartilage erosion was scored on a scale of 0–4, where 0 = no destruction, 1 = minimal erosion limited to single spots, 2 = slight to moderate erosion in a limited area, 3 = more extensive areas of erosion, and 4 = general destruction.

Weight measurements

Arthritic mice were injected IP with carrier control or with SAV prodrug at dosages ranging from 0.083 mg/kg/day to 2.25 mg/kg/day for 10 days, except in mice receiving 2.25 mg/kg/day of SAV, which only received 4 days of IP injections. Mice were weighed every other day. Group results were then normalized to the group weight at the beginning of the experiment.

Protease imaging

The protease imaging technique has been described in detail previously (25). Briefly, a protease-activatable probe (2 n*M* ProSense 680; VisEn Medical, Bedford, MA) was injected into mice on day 9 of serum-transfer arthritis. Imaging was performed on a reflectance fluorescence system (model OV100; Olympus, Lake Success, NY) using a 715–755-nm excitation filter and a 780–855-nm emission filter. Mice were imaged the day following probe injection, while under inhalation anesthesia. Exposure times were constant across all images. Region of interest markers were placed over the ankles, and the total fluorescence intensity was measured. Image analysis was performed using ImageJ software (NIH Image, National Institutes of Health, Bethesda, MD; online at: http://rsbweb.nih.gov/ij/).

Anti–glucose-6-phosphate isomerase (anti-GPI) ELISA

The anti-GPI ELISA has been described elsewhere (26). Briefly, recombinant GPI was coated on ELISA plates at 5 μg/μl, and diluted sera were applied. Anti-GPI IgG was detected with alkaline phosphatase–conjugated anti-mouse IgG and alkaline phosphate substrate at 405 nm.

Confocal imaging of vessel permeability

Confocal microscopy has previously been described in detail (27). Briefly, microscopy was performed with a multichannel upright confocal microscope (Radiance 2100; Bio-Rad, Richmond, CA). The 637-nm red-laser diode was used for excitation, and images were acquired through a 660-nm long-pass filter. Mice were injected IP with SAV or carrier control at a dosage of 0.75 mg/kg for 3 days prior to imaging. They were anesthetized with inhalational isoflurane, and 100 μl of a macromolecular vascular probe (AngioSense 680; VisEn) was injected intravenously. Imaging was then initiated in order to acquire baseline (pre–serum injection) images. After 5 minutes, 200 μl of serum was injected intravenously, and imaging data were collected continuously. Time-lapse movies were created by obtaining images every 3 seconds, permitting assessment of vascular leakage over time. Quantification was performed using ImageJ image analysis software by calculating the mean fluorescence intensity of each field of view. Calculation of the maximum rate of leakage was performed via a custom-written software program using S-Plus (Tibco, Palo Alto, CA).

Imaging of neutrophil–endothelium interactions

The imaging of neutrophil–endothelium interactions has been described in detail elsewhere (28). Briefly, isolation of mature neutrophils from bone marrow was accomplished using discontinuous Percoll density centrifugation. Neutrophils were labeled with a fluorescent dye (20 μ*M* CellTracker Green CMFDA [488 nm excitation and 530 nm emission spectra]; Invitrogen, San Diego, CA) and were injected retroorbitally into arthritic B6 mice 6 days after serum transfer. A vascular probe was injected (AngioSense 750 [750 nm excitation and

780 nm emission spectra]; VisEn Medical) to help delineate the capillaries. Interactions of neutrophils with the ankle vasculature were imaged using laser-scanning time-lapse microscopy ~60 minutes after neutrophil injection (Olympus IV-100 instrument). Immediately before imaging, the paw and ankle skin was removed to permit increased clarity of visualization. Images were randomly collected over the ventral aspect of the paw and ankle. Videos were acquired for 30 seconds. Stationary neutrophils were visualized and scored in sequential time-series images. SAV and carrier control were administered at a dosage of 0.75 mg/kg 3 days prior to imaging.

Flow cytometry

Primary murine lung endothelial cells were seeded at a density of 10^5 cells/well in Dulbecco's modified Eagle's medium supplemented with 20% fetal calf serum, 1% penicillin/streptomycin, 1% nonessential amino acids, 1% sodium pyruvate, 1 m*M* L-glutamine, 2 μg/ml of endothelial mitogen, and 0.1 mg/ml of heparin. After 24 hours, SAV (10 μ*M*) was added to appropriate groups. Twelve hours later, murine TNFα (10 ng/ml) was added to appropriate groups. Cells were harvested via nonenzymatic detachment 2 hours after the last treatment. Cells were labeled with antibodies directed against CD31, CD34, and vascular cell adhesion molecule 1 (VCAM-1; BD PharMingen, San Diego, CA), and flow cytometry was performed. Endothelial cells were identified as CD31+ and CD34+, and the VCAM signal was measured in double-positive cells.

Neutrophil burst assay

Mice were injected IP with SAV or carrier control for 3 days prior to the neutrophil burst assay at a dosage of 0.75 mg/kg. Neutrophils were isolated as described above. The production of reactive oxygen species was measured by a luminol-dependent and horseradish peroxidase–dependent chemiluminescence assay. All procedures were carried out at 37°C in Dulbecco's phosphate buffered saline (DPBS) with calcium and magnesium. Neutrophils (5×10^6/ml) were primed for 20 minutes at 37°C with 100 ng/ml of mouse TNFα (R&D Systems, Minneapolis, MN). Afterward, 100 μl of prewarmed DPBS or plain wortmannin (to the indicated final concentrations), with horseradish peroxidase and luminol (20 units/ml and 150 μ*M* final concentrations, respectively) was added to 100-μl aliquots of primed cells, which had been preincubated for 3 minutes.

Duplicate aliquots (150 μl) were transferred to a prewarmed 96-well plate, stimuli (50 μl) were added manually, and chemiluminescence was followed over time using a Centro LB 960 luminometer (Berthold Technologies, Oak Ridge, TN). Formyl-Met-Leu-Phe (fMLP) and phorbol myristate acetate (PMA) were used at a final concentration of 10 μ*M* and 100 ng/ml, respectively. Data output was expressed in relative light units per second, and total integrated reactive oxygen species production was calculated as the area under the curve.

Neutrophil degranulation assay

Prior to the assay, mice were injected IP with SAV or carrier control for 3 days at a dosage of 0.75 mg/kg. Neutrophils were isolated as described above, pooling neutrophils from 3 mice per group. Neutrophil degranulation was investigated by measuring the absorbance (at 405 nm) of a colorimetric elastase substrate (methoxysuccinyl-alanine-alanine-proline-valine-paranitroanilide). One hundred microliters of a neutrophil suspension (5×10^6 cell/ml), 10 μl of cytochalasin B (0.1 mg/ml), and 20 μl of Hanks' balanced salt solution (HBSS) were incubated for 10 minutes at 37°C. Then, 20 μl of elastase substrate (1 mg/ml) was added. Next, 20 μl of fMLP (10 μ*M*) or PMA (0.3 μ*M*) was added, and the change in mean optical density was recorded over the next 15 minutes. Blank wells contained no fMLP or PMA and an additional 20 μl of HBSS. Three independent experiments were performed, each of which was run in triplicate.

Statistical analysis

Statistical analysis was performed using the software program Prism 4c (GraphPad Software, San Diego, CA). One-way analysis of variance (ANOVA) and Student's *t*-test were performed where appropriate. *P* values less than 0.05 were considered significant.

RESULTS

Prevention and treatment of serum-transfer arthritis with SAV

To determine whether SAV had any effect on inflammatory arthritis, we tested it in the K/BxN serum–transfer model of arthritis. In the prevention experiments, we aimed to modify disease progression by coinjecting SAV at the time of arthritis induction. A dosage of 0.75 mg/kg completely protected the mice from joint swelling (Figure 2A). A 3-fold lower dosage also had a significant effect, with an ~50% reduction in ankle thickening. A dosage of 0.083 mg/kg still resulted in a detectable and significant decrease in joint swelling.

These findings were corroborated by analysis of histologic sections. Ankles of control mice were highly inflamed, with gross invasion of leukocytes in the connective tissue and joints and thickening of the synovial lining, whereas ankles of mice treated with SAV at a dosage of 0.75 mg/kg appeared normal, without any features of inflammation (Figure 2B). We found a linear response to the SAV compound for the inflammation score ($r^2 = 0.87$). A dosage of 0.75 mg/kg led to the greatest reduction in inflammation. The other 2 dosages showed less pronounced, but considerable, reductions in inflammation scores (Figure 2C). There also was significant reduction in the cartilage erosion score. A graded response was not detected, however, because of the low level of cartilage erosion in the control group (Figure 2D). These experiments established 0.75 mg/kg as a highly effective dose.

Next, in an interventional approach, we sought to test whether the compound was effective in modifying active and progressing arthritis, a possibly more challenging scenario. Arthritis was induced by injection of K/BxN mouse serum on day 0; on day 6, treatment with control or SAV was started. On day 8, there was a notable separation between the 2 groups. Arthritis progressed in the control group, whereas the SAV-treated mice displayed reduced ankle thickness as compared with the control group (Figure 2E) on day 6. On day 10, this effect was even more pronounced, with a 50% reduction of joint swelling in the mice treated with 0.75 mg/kg of SAV (Figure 2E).

We tested for weight loss, a potential adverse side effect that has been described with the inhibition of PI3Ks. There was no difference between the control group and the experimental groups at dosages of up to 0.75 mg/kg. Only by increasing by a factor of 3 (to 2.25 mg/kg) the dosage that gave a maximum inhibitory effect were detectable differences in weight demonstrated (Figure 2F); these effects were reversible. No mouse died during any experiment.

Reduction of protease activity by SAV treatment

Protease activity has been shown to be an early indicator of the inflammation of arthritis (25). We used an imaging-based approach to assess protease activity. In the prevention experiment, there was a graded dose-response to SAV (Figure 3A). There was a 22% decrease in the mice receiving the lowest dosage and a 30% decrease in those receiving the medium dosage as compared with control mice. The highest dosage almost completely abrogated protease activity as compared with background levels (Figure 3B). There was a high degree of correlation between ankle swelling and protease activity ($r^2 = 0.86$) (Figure 3C). We also performed protease imaging in the intervention setting. Interestingly, protease activity was reduced by 79% (Figure 3B), whereas ankle thickness was diminished by only

50%. This discrepancy points to a faster response of protease activity to treatment as compared with edematous swelling.

SAV-induced amelioration of arthritis in K/BxN mice during the effector phase

The K/BxN model is characterized by a more severe and destructive form of arthritis than is usually seen with the serum-transfer system, and this is driven by constantly higher titers of the relevant autoantibody, anti-GPI. In the prevention experiments, K/BxN mice were given SAV or carrier control prior to any signs of joint swelling. Control mice developed a profound swelling, measuring ~0.9 mm, with a rapid onset around day 35. SAV-treated mice displayed only a mild increase in ankle thickness of ~0.1 mm (Figure 4A). This antiinflammatory effect was present until SAV treatment was discontinued, after which the SAV-treated mice developed the same amount of swelling as the control mice and with a similar onset, indicating that the antiinflammatory effect of SAV was neither permanent nor irreversible.

One possible effect of SAV is that it alters the amount of circulating anti-GPI antibodies, which are the etiologic stimulus in this model. Therefore, we measured antibody titers during the disease control phase and after the mice had developed complete ankle swelling. There was virtually no difference at the 2 time points, indicating that SAV interfered with arthritis downstream of antibody production (Figure 4B).

Compromised endothelial cell function in SAV-treated mice

Rapid changes in endothelial permeability after injection of K/BxN serum have been shown to promote arthritis (27). We consequently analyzed early leakage and found a moderately diminished leak response in SAV-treated mice (Figure 5A). There was a 13% reduction in the final leak response at 10 minutes after injection of K/BxN serum (Figure 5B). The maximum rate of leakage was decreased by one-third (Figure 5C).

Since the endothelium is important in leukocyte extravasation, we investigated whether the administration of SAV had an effect on the capture of neutrophils by imaging ex vivo–labeled neutrophils and analyzing their movement and attachment behaviors. Mice that received carrier and serum showed 14.4 ± 1.2 stationary neutrophils/high-power field (hpf) (mean ± SEM), whereas those that received carrier but no serum showed only 4.8 ± 0.7 stationary neutrophils/hpf. We then examined mice that had been treated with SAV, performing 2 experiments to distinguish the effects of SAV on neutrophils and endothelium. We detected 15.2 ± 1.4 stationary neutrophils/hpf in SAV-treated donor mice, whereas in SAV-treated recipient mice, this value dropped to 5.6 ± 0.9 stationary neutrophils/hpf (Figures 5D and E). A one-way ANOVA showed these differences to be statistically significant.

We then investigated whether the dysfunctional endothelial activation was a direct or indirect effect of SAV. Endothelial cells treated with SAV or carrier and then stimulated with TNFα were analyzed by flow cytometry for the presence of VCAM. The addition of SAV reduced the baseline VCAM signal by 47.2%, whereas activation of endothelial cells by TNFα increased the VCAM signal by 35.5%. Addition of SAV to TNFα-activated cells prevented the VCAM signal increase, instead reducing it by 32.5% compared with baseline (Figure 5F).

Impaired neutrophil oxidative burst and degranulation in SAV-treated mice

Neutrophils are a driving force in K/BxN serum–transfer arthritis. Hence, we investigated whether SAV had an effect on neutrophil functionality. Neutrophils from SAV-treated mice displayed a drastically different oxidative burst as compared with untreated controls when

the production of reactive oxygen species was triggered by fMLP, a PI3K-dependent stimulus (Figure 6A). The response was slower and less intense. The area under the curve was reduced by 59% (n = 4 mice) (data not shown). In contrast, neutrophils prepared in the same manner showed no difference as compared with controls when the oxidative burst was induced by PMA, a PI3K-independent stimulus (Figure 6B).

This oxidative burst assay allowed us to calculate the bioactive concentration of wortmannin provided by SAV. A dose-response curve of plain wortmannin was generated and set in relation to SAV-related burst inhibition. A SAV dosage of 0.75 mg/kg provided ~41 n*M* bioactive wortmannin (Figure 6C). Since we found a decrease in protease activity in SAV-treated mice, we investigated whether degranulation was impaired. Indeed, there was a 47% decrease in degranulation when triggered by fMLP (Figure 6D). PMA-induced degranulation was not altered (data not shown).

DISCUSSION

It has been conclusively established that PI3Ks play an integral role in the pathogenesis of inflammatory arthritis (14). PI3Ks are intracellular elements of a dysregulated self-perpetuating cytokine network whose extracellular members include TNFα and IL-1. The success of therapies directed against these molecules points to the importance of this network in RA. Therefore, the development of agents such as SAV, which target PI3K signaling, is highly desirable.

In the present study, we evaluated the effects of a recently developed self-activating viridin prodrug that slowly releases wortmannin on inflammatory arthritis (22,23,29). We hypothesized that it might have a potent antiinflammatory capacity, given the reported inhibition of all isoforms of PI3Ks and other kinases by wortmannin (31), as well as the enhanced and temporally extended delivery of wortmannin by the SAV prodrug. Indeed, we found that SAV was able to greatly reduce joint swelling in the original K/BxN model and to prevent joint swelling in the K/BxN serum–transfer model. Other parameters of inflammation were also dramatically reduced. Histologic examination of arthritic paws showed only weak signs of inflammation, and no signs of cartilage erosion. An imaging-based analysis of protease activity revealed signals that were minimally elevated above background.

We then tested SAV in an interventional setting, which more closely resembles the condition in humans, since RA patients present with symptoms. The compound was highly efficacious as a treatment, reducing joint swelling and protease activity to a large extent.

Although PI3Ks have been implicated in multiple T cell– and B cell–mediated processes (15–20), we could not detect a dysfunction in these populations at the autoantibody level, since the titers of anti-GPI antibody were unchanged between treated mice in which the arthritis was clinically controlled and in the same mice after termination of SAV administration. This finding, coupled with the potent effect of SAV in the serum-transfer model, points to a mechanism that lies down-stream of autoantibody synthesis.

An early event after injection of anti-GPI antibodies is macromolecular leakage. Neutrophils, mast cells, and endothelial cells are involved in this phenomenon (27). Anti-GPI is recognized by neutrophils, which subsequently release TNFα. Mast cells respond by releasing histamine, which leads to increased vascular permeability, allowing more anti-GPI antibodies to leave the circulation and be deposited in the joints. More inflammatory cells can also access the region. The importance of this phenomenon is demonstrated by the reduced arthritis in leakage-deficient mice (27). We found a moderate decrease in total

leakage and a more profound decrease in the leakage rate in SAV-treated mice, indicating that SAV had an effect on leak-effector cells.

Mast cells rely on PI3K signaling for histamine release after stimulation (31), and PI3K-knockout mice have been reported to show disturbed allergic mast cell–dependent responses (12,13). The findings of the present study are corroborated by a study showing that a PI3Kδ-specific inhibitor reduced vascular permeability in an asthma model (32). It is thus conceivable that mast cells are affected by SAV.

Endothelial cells are also affected and likely contribute to the decreased vascular permeability. It was previously shown that VEGF-induced loss of the blood–brain barrier in an ischemic event occurred in a mast cell–independent manner. VEGF increased leakage, and this effect was reversed by wortmannin (33). We showed that neutrophils exhibit impaired degranulation and, thus, impaired release of TNFα after SAV treatment. We cannot, however, quantify the relative contribution of the several effectors in the reduction of leakage after SAV administration.

Neutrophils are a driving force of arthritis in the K/BxN model. They are the most abundant cells in the inflamed joint and are crucial to disease progression because of protease and cytokine release (34). Their role is best exemplified by the fact that neutrophil-depleted mice are protected from arthritis (35). We found a strong inhibition of several neutrophil functions. The oxidative burst was profoundly impaired. This burst, however, is not needed for arthritis initiation and progression (35). Degranulation of protease-laden vesicles was also reduced by one-half, which is consistent with the decreased protease activity detected by imaging analyses. Our experiments clearly indicate the interaction of SAV with PI3K-dependent cellular functions. SAV inhibited degranulation and burst only if these functions were triggered by fMLP, a PI3K-dependent stimulus, whereas SAV treatment had no effect on PMA-stimulated responses (7).

We found fewer neutrophils infiltrating the joint and synovium in SAV-treated mice. It is possible that neutrophils were not properly recruited to the site of inflammation. To investigate this possibility, we performed an imaging study examining firm neutrophil attachment to the endothelium, an early step in leukocyte extravasation. SAV treatment of donor neutrophils had no impact on attachment. This finding was counterintuitive, since previous studies showed that neutrophils rely on PI3Ks in order to extravasate (7,9). However, it was recently demonstrated that firm neutrophil attachment is not altered in PI3Kδ-deficient mice or in mice treated with a PI3Kδ-specific inhibitor (36). SAV administration to recipient mice, though, and thus to structures such as the endothelium, reduced the number of attached neutrophils almost to baseline levels. Endothelial cells express PI3K isoforms, which are required for successful leukocyte capture and extravasation, since inhibition of their function decreases trafficking into inflamed tissues (36,37). We also found a direct inhibition of endothelial cells by SAV: SAV-treated endothelial cells did not respond to TNFα treatment by upregulating membrane-bound VCAM, a surrogate marker of activation of inflammatory cells. This observation, along with previous findings, indicates that endothelial cells rely at least partly on PI3K signaling to allow leukocyte diapedesis (36,37).

There are further potential mechanisms of action that could not be addressed in this study. IL-10 is a potent antiinflammatory cytokine that plays an important role in the control of RA (38). Several studies have investigated the impact of PI3K inhibition, using agents such as wortmannin or LY294002, on IL-10 production and found contradictory results. Some studies showed up-regulation and, thus, an enhanced antiinflammatory profile (39), while others demonstrated down-regulation and, thus, a more proinflammatory effect (40). It is

conceivable that SAV exerts its antiinflammatory activity to some degree through IL-10, but given the apparent complexity of IL-10 regulation, it is difficult to predict whether this is true. Further investigation is warranted to answer this question.

FoxOa3, a PI3K downstream target, was recently reported to be crucial in maintaining arthritis by preventing neutrophils from TNFα–induced and IL-1–induced apoptosis (41). This observation is interesting with respect to our findings, since one would expect SAV to inhibit PI3Ks and thus cause activation of FoxOa3 and increased resistance of neutrophils to apoptosis. It should allow them to survive in inflammatory environments and to entertain arthritis. This was not the case in our study. The discrepancy might be due to the fact that the above-mentioned study tested for FoxOa3 inhibition directly, while we investigated targets further upstream of FoxOa3. The overall effect, however, despite potentially enhanced resistance of neutrophils to apoptosis, was an almost complete abrogation of arthritis. It seems that other downstream effects of SAV counteract FoxOa3 and its actions.

Finally, the findings of our study are specific to the K/BxN model. We chose this model for its high degree of reproducibility and penetrance. Collagen-induced arthritis, for example, has only ~70% penetrance (42). As a unique feature, the K/BxN model also allows for separation of the autoimmune initiation phase and the inflammatory effector phase. Due to the inherent shortcomings of any model, we cannot predict the validity of our findings in other animal models or in human disease, but we think that our results provide a legitimate expectation that SAV might be a valuable therapeutic agent.

In summary, we demonstrated the antiinflammatory activity of a novel self-activating viridin prodrug in a model of inflammatory arthritis. This compound releases wortmannin, which is known to inhibit PI3K, among other enzymes. SAV is superior to wortmannin itself because of its enhanced slow-release profile (23,43). We found pleiotropic effects of the drug, including effects on neutrophils and endothelial activation, which combined to yield complete protection from joint disease.

Acknowledgments

Supported in part by NIH grants P01-AI-054904, R01-EB-001872, R01-AR-046580, R24-CA-92782, and P50-CA-86355.

REFERENCES

1. Horai R, Saijo S, Tanioka H, Nakae S, Sudo K, Okahara A, et al. Development of chronic inflammatory arthropathy resembling rheumatoid arthritis in interleukin 1 receptor antagonist-deficient mice. J Exp Med. 2000; 191:313–320. [PubMed: 10637275]
2. Bresnihan B, Alvaro-Gracia JM, Cobby M, Doherty M, Domljan Z, Emery P, et al. Treatment of rheumatoid arthritis with recombinant human interleukin-1 receptor antagonist. Arthritis Rheum. 1998; 41:2196–2204. [PubMed: 9870876]
3. Keffer J, Probert L, Cazlaris H, Georgopoulos S, Kaslaris E, Kioussis D, et al. Transgenic mice expressing human tumour necrosis factor: a predictive genetic model of arthritis. EMBO J. 1991; 10:4025–4031. [PubMed: 1721867]
4. Elliott MJ, Maini RN, Feldmann M, Kalden JR, Antoni C, Smolen JS, et al. Randomised double-blind comparison of chimeric monoclonal antibody to tumour necrosis factor α (cA2) versus placebo in rheumatoid arthritis. Lancet. 1994; 344:1105–1110. [PubMed: 7934491]
5. Lipsky PE, van der Heijde DM, St. Clair EW, Furst DE, Breedveld FC, Kalden JR, et al. for the Anti–Tumor Necrosis Factor Trial in Rheumatoid Arthritis with Concomitant Therapy Study Group. Infliximab and methotrexate in the treatment of rheumatoid arthritis. N Engl J Med. 2000; 343:1594–1602. [PubMed: 11096166]

6. Weinblatt ME, Kremer JM, Bankhurst AD, Bulpitt KJ, Fleischmann RM, Fox RI, et al. A trial of etanercept, a recombinant tumor necrosis factor receptor:Fc fusion protein, in patients with rheumatoid arthritis receiving methotrexate. N Engl J Med. 1999; 340:253–259. [PubMed: 9920948]
7. Hirsch E, Katanaev VL, Garlanda C, Azzolino O, Pirola L, Silengo L, et al. Central role for G protein-coupled phosphoinositide 3-kinase γ in inflammation. Science. 2000; 287:1049–1053. [PubMed: 10669418]
8. Li Z, Jiang H, Xie W, Zhang Z, Smrcka AV, Wu D. Roles of PLC-β2 and -β3 and PI3Kγ in chemoattractant-mediated signal transduction. Science. 2000; 287:1046–1049. [PubMed: 10669417]
9. Sasaki T, Irie-Sasaki J, Jones RG, Oliveira-dos-Santos AJ, Stanford WL, Bolon B, et al. Function of PI3Kγ in thymocyte development, T cell activation, and neutrophil migration. Science. 2000; 287:1040–1046. [PubMed: 10669416]
10. Clayton E, Bardi G, Bell SE, Chantry D, Downes CP, Gray A, et al. A crucial role for the p110δ subunit of phosphatidylinositol 3-kinase in B cell development and activation. J Exp Med. 2002; 196:753–763. [PubMed: 12235209]
11. Okkenhaug K, Bilancio A, Farjot G, Priddle H, Sancho S, Peskett E, et al. Impaired B and T cell antigen receptor signaling in p110δ PI 3-kinase mutant mice. Science. 2002; 297:1031–1034. [PubMed: 12130661]
12. Ali K, Bilancio A, Thomas M, Pearce W, Gilfillan AM, Tkaczyk C, et al. Essential role for the p110δ phosphoinositide 3-kinase in the allergic response. Nature. 2004; 431:1007–1011. [PubMed: 15496927]
13. Laffargue M, Calvez R, Finan P, Trifilieff A, Barbier M, Altruda F, et al. Phosphoinositide 3-kinase γ is an essential amplifier of mast cell function. Immunity. 2002; 16:441–451. [PubMed: 11911828]
14. Camps M, Rueckle T, Ji H, Ardissone V, Rintelen F, Shaw J, et al. Blockade of PI3Kγ suppresses joint inflammation and damage in mouse models of rheumatoid arthritis. Nat Med. 2005; 11:936–943. [PubMed: 16127437]
15. Randis T, Puri K, Zhou H, Diacovo T. Role of PI3Kγ and PI3Kδ in inflammatory arthritis and tissue localization of neutrophils. Eur J Immunol. 2008; 38:1215–1224. [PubMed: 18412166]
16. Arcaro A, Wymann MP. Wortmannin is a potent phosphatidylinositol 3-kinase inhibitor: the role of phosphatidylinositol 3,4,5-trisphosphate in neutrophil responses. Biochem J. 1993; 296:297–301. [PubMed: 8257416]
17. Knight ZA, Gonzalez B, Feldman ME, Zunder ER, Goldenberg DD, Williams O, et al. A pharmacological map of the PI3-K family defines a role for p110α in insulin signaling. Cell. 2006; 125:733–747. [PubMed: 16647110]
18. Wymann MP, Bulgarelli-Leva G, Zvelebil MJ, Pirola L, Vanhae-sebroeck B, Waterfield MD, et al. Wortmannin inactivates phosphoinositide 3-kinase by covalent modification of Lys-802, a residue involved in the phosphate transfer reaction. Mol Cell Biol. 1996; 16:1722–1733. [PubMed: 8657148]
19. Walker EH, Pacold ME, Perisic O, Stephens L, Hawkins PT, Wymann MP, et al. Structural determinants of phosphoinositide 3-kinase inhibition by wortmannin, LY294002, quercetin, myricetin, and staurosporine. Mol Cell. 2000; 6:909–919. [PubMed: 11090628]
20. Wiesinger D, Gubler HU, Haefliger W, Hauser D. Antiinflammatory activity of the new mould metabolite 11-desacetoxy-wortmannin and of some of its derivatives. Experientia. 1974; 30:135–136. [PubMed: 4814585]
21. Vanhaesebroeck B, Leevers SJ, Ahmadi K, Timms J, Katso R, Driscoll PC, et al. Synthesis and function of 3-phosphorylated inositol lipids. Annu Rev Biochem. 2001; 70:535–602. [PubMed: 11395417]
22. Yuan H, Luo J, Weissleder R, Cantley L, Josephson L. Wortmannin-C20 conjugates generate wortmannin. J Med Chem. 2006; 49:740–747. [PubMed: 16420059]
23. Blois J, Yuan H, Smith A, Pacold ME, Weissleder R, Cantley LC, et al. Slow self-activation enhances the potency of viridin prodrugs. J Med Chem. 2008; 51:4699–4707. [PubMed: 18630894]

24. Kouskoff V, Korganow AS, Duchatelle V, Degott C, Benoist C, Mathis D. Organ-specific disease provoked by systemic autoimmunity. Cell. 1996; 87:811–822. [PubMed: 8945509]
25. Ji H, Ohmura K, Mahmood U, Lee DM, Hofhuis FM, Boackle SA, et al. Arthritis critically dependent on innate immune system players. Immunity. 2002; 16:157–168. [PubMed: 11869678]
26. Matsumoto I, Staub A, Benoist C, Mathis D. Arthritis provoked by linked T and B cell recognition of a glycolytic enzyme. Science. 1999; 286:1732–1735. [PubMed: 10576739]
27. Binstadt BA, Patel PR, Alencar H, Nigrovic PA, Lee DM, Mahmood U, et al. Particularities of the vasculature can promote the organ specificity of autoimmune attack. Nat Immunol. 2006; 7:284–292. [PubMed: 16444258]
28. Wu HJ, Sawaya H, Binstadt B, Brickelmaier M, Blasius A, Gorelik L, et al. Inflammatory arthritis can be reined in by CpG-induced DC–NK cell cross talk. J Exp Med. 2007; 204:1911–1922. [PubMed: 17646407]
29. Yuan H, Barnes KR, Weissleder R, Cantley L, Josephson L. Covalent reactions of wortmannin under physiological conditions. Chem Biol. 2007; 14:321–328. [PubMed: 17379147]
30. Bain J, Plater L, Elliott M, Shpiro N, Hastie CJ, McLauchlan H, et al. The selectivity of protein kinase inhibitors: a further update. Biochem J. 2007; 408:297–315. [PubMed: 17850214]
31. Rommel C, Camps M, Ji H. PI3Kδ and PI3Kγ: partners in crime in inflammation in rheumatoid arthritis and beyond? Nat Rev Immunol. 2007; 7:191–201. [PubMed: 17290298]
32. Lee KS, Park SJ, Kim SR, Min KH, Jin SM, Puri KD, et al. Phosphoinositide 3-kinase-δ inhibitor reduces vascular permeability in a murine model of asthma. J Allergy Clinical Immunol. 2006; 118:403–409. [PubMed: 16890765]
33. Kilic E, Kilic U, Wang Y, Bassetti CL, Marti HH, Hermann DM. The phosphatidylinositol-3 kinase/Akt pathway mediates VEGF's neuroprotective activity and induces blood brain barrier permeability after focal cerebral ischemia. FASEB J. 2006; 20:1185–1187. [PubMed: 16641198]
34. Chen M, Lam BK, Kanaoka Y, Nigrovic PA, Audoly LP, Austen KF, et al. Neutrophil-derived leukotriene B4 is required for inflammatory arthritis. J Exp Med. 2006; 203:837–842. [PubMed: 16567388]
35. Wipke BT, Allen PM. Essential role of neutrophils in the initiation and progression of a murine model of rheumatoid arthritis. J Immunol. 2001; 167:1601–1608. [PubMed: 11466382]
36. Puri KD, Doggett TA, Douangpanya J, Hou Y, Tino WT, Wilson T, et al. Mechanisms and implications of phosphoinositide 3-kinase δ in promoting neutrophil trafficking into inflamed tissue. Blood. 2004; 103:3448–3456. [PubMed: 14751923]
37. Puri KD, Doggett TA, Huang CY, Douangpanya J, Hayflick JS, Turner M, et al. The role of endothelial PI3Kγ activity in neutrophil trafficking. Blood. 2005; 106:150–157. [PubMed: 15769890]
38. Katsikis PD, Chu CQ, Brennan FM, Maini RN, Feldmann M. Immunoregulatory role of interleukin 10 in rheumatoid arthritis. J Exp Med. 1994; 179:1517–1527. [PubMed: 8163935]
39. Williams DL, Li C, Ha T, Ozment-Skelton T, Kalbfleisch JH, Preiszner J, et al. Modulation of the phosphoinositide 3-kinase pathway alters innate resistance to polymicrobial sepsis. J Immunol. 2004; 172:449–456. [PubMed: 14688354]
40. Foey A, Green P, Foxwell B, Feldmann M, Brennan F. Cytokine-stimulated T cells induce macrophage IL-10 production dependent on phosphatidylinositol 3-kinase and p70S6K: implications for rheumatoid arthritis. Arthritis Res. 2002; 4:64–70. [PubMed: 11879539]
41. Jonsson H, Allen P, Peng S. Inflammatory arthritis requires FoxOa3 to prevent Fas ligand-induced neutrophil apoptosis. Nat Med. 2005; 11:666–671. [PubMed: 15895074]
42. Kannan K, Ortmann RA, Kimpel D. Animal models of rheumatoid arthritis and their relevance to human disease. Pathophysiology. 2005; 12:167–181. [PubMed: 16171986]
43. Zask A, Kaplan J, Toral-Barza L, Hollander I, Young M, Tischler M, et al. Synthesis and structure-activity relationships of ringopened 17-hydroxywortmannins: potent phosphoinositide 3-kinase inhibitors with improved properties and anticancer efficacy. J Med Chem. 2008; 51:1319–1323. [PubMed: 18269228]

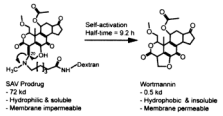

Figure 1.

Chemical structure of the self-activating viridin (SAV) prodrug. Arrow shows slow self-activation, which slowly generates wortmannin, the active viridin. SAV in the inactive state contains a 70-kd dextran carrier and, thus, attains many of the physical and biologic properties of dextran, including approximate size, hydrophilicity, and poor cell penetration. After self-activation, wortmannin rapidly enters cells and inhibits phosphatidylinositol 3-kinase, among other kinases. SAV is a lyophilized powder, and activation begins with the addition of phosphate buffered saline and continues in plasma. The slow self-activation enhances its potency and produces low, sustained levels of wortmannin.

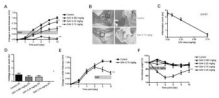

Figure 2.

Effects of self-activating viridin (SAV) on serum-transfer arthritis. **A**, Dose-dependent prevention of ankle swelling after induction of arthritis by injection of K/BxN mouse serum. SAV treatment (shaded bar) at the indicated concentrations was started at the time of arthritis induction. **B**, Representative histologic sections of ankle joints from a control mouse and a mouse treated with high-dose SAV. The section from the control mouse shows a highly inflamed ankle, with joint and soft tissue invasion of leukocytes, whereas the section from the SAV-treated mouse is similar to that of a mouse in which arthritis has not been induced (results not shown). Images at the right are higher-magnification views (original magnification × 100) of the boxed areas in the images at the left (original magnification × 20). **C**, Histologic scores for inflammation in mice with serum-transfer arthritis. There was a linear reduction of features of inflammation at the 3 concentrations of SAV used. **D**, Histologic scores for cartilage erosion in mice with serum-transfer arthritis. High-dose SAV prevented cartilage destruction. **E**, Intervention experiment with SAV treatment in progressing serum-transfer arthritis. There was a sharp response to administration of SAV (shaded bar), with reversal of ankle swelling. **F**, Effect of SAV treatment on weight. Only the group given 2.25 mg/kg of SAV (shaded bar) showed a significant difference from the controls. The weight loss was reversible, with animals regaining weight after cessation of SAV treatment. Values are the mean ± SEM of 5 mice per group in **A**, **E**, and **F**, and of 3–4 mice per group in **C** and **D**. * = $P < 0.05$; ** = $P < 0.001$ versus controls.

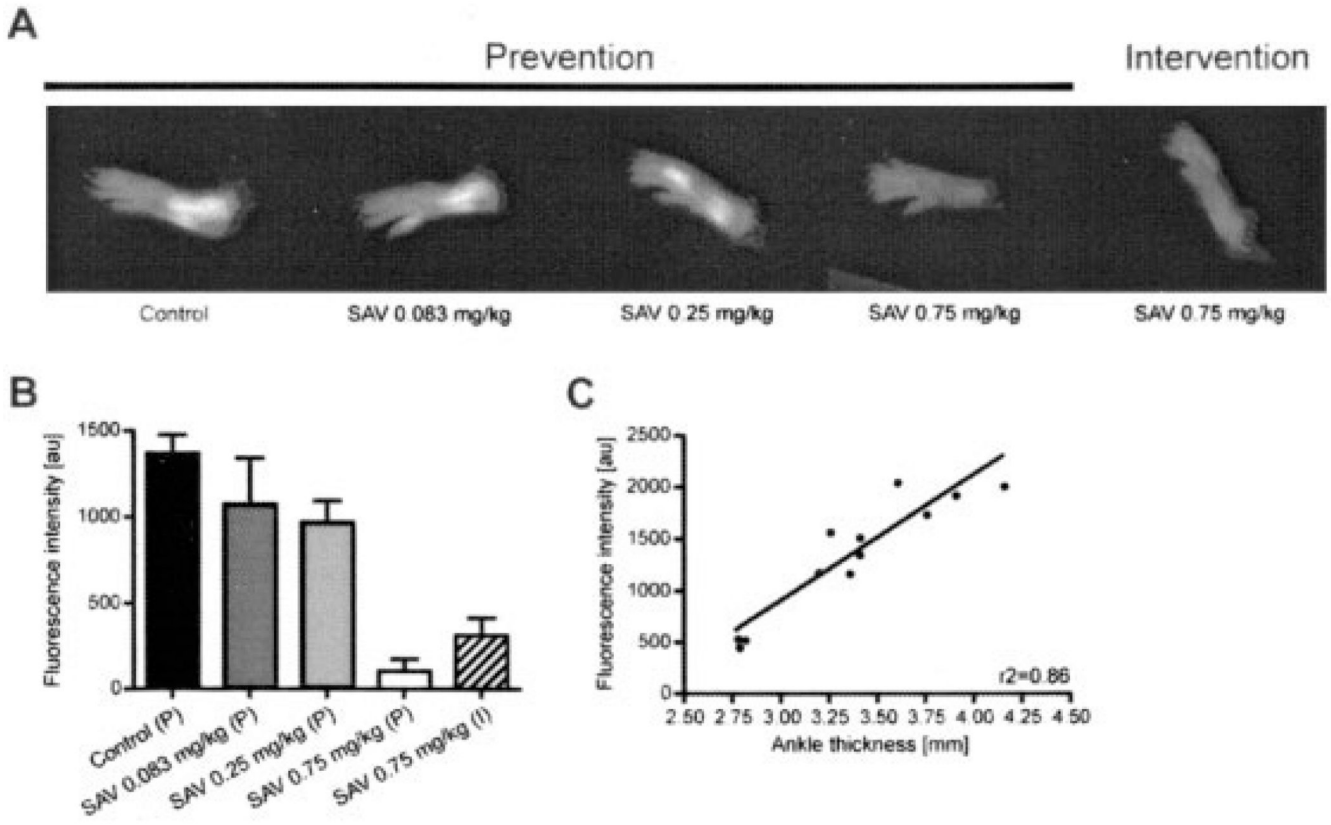

Figure 3.

Reduction of protease activity by self-activating viridin (SAV) treatment in the serum-transfer model of arthritis. **A**, Representative near-infrared images of protease activity in the prevention and intervention experiments. A protease-activatable fluorescent probe was injected 24 hours prior to imaging. A dose-dependent decrease in protease activity with SAV treatment in the prevention experiments can be seen. SAV also reduced protease activity in the interventional experiment. **B**, Quantification of results from the protease activity imaging studies. Region of interest makers were placed over ankles, and the mean fluorescence intensity (in arbitrary units [AU]) was measured. There was an apparent reduction of protease activity with increasing dosages of SAV. Values are the mean and SEM of 3–4 mice per group. **C**, Correlation between ankle thickness and protease activity in prevention experiments with SAV treatment. There was a high degree of correlation between ankle swelling and protease activity (n = 12 mice).

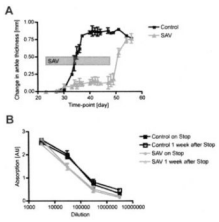

Figure 4.

Effects of self-activating viridin (SAV) treatment in K/BxN mice. **A**, SAV treatment (shaded bar) was started before the spontaneous onset of arthritic ankle swelling in K/BxN mice. SAV controlled the arthritis, as indicated by the low levels of ankle swelling in treated mice. Soon after cessation of SAV administration, the mice developed arthritis. **B**, Titers of anti–glucose-6-phosphate isomerase (anti-GPI), the driving pathogenetic agent of the arthritis in K/BxN mice, were not changed by SAV treatment. Anti-GPI antibody titers were measured during the disease control phase and after the mice had developed complete ankle swelling. Results are expressed as the absorbance at 405 nm (in arbitrary units [AU]), as determined by enzyme-linked immunosorbent assay. On stop represents the time treatment was stopped. Values are the mean ± SEM of 5 mice per group.

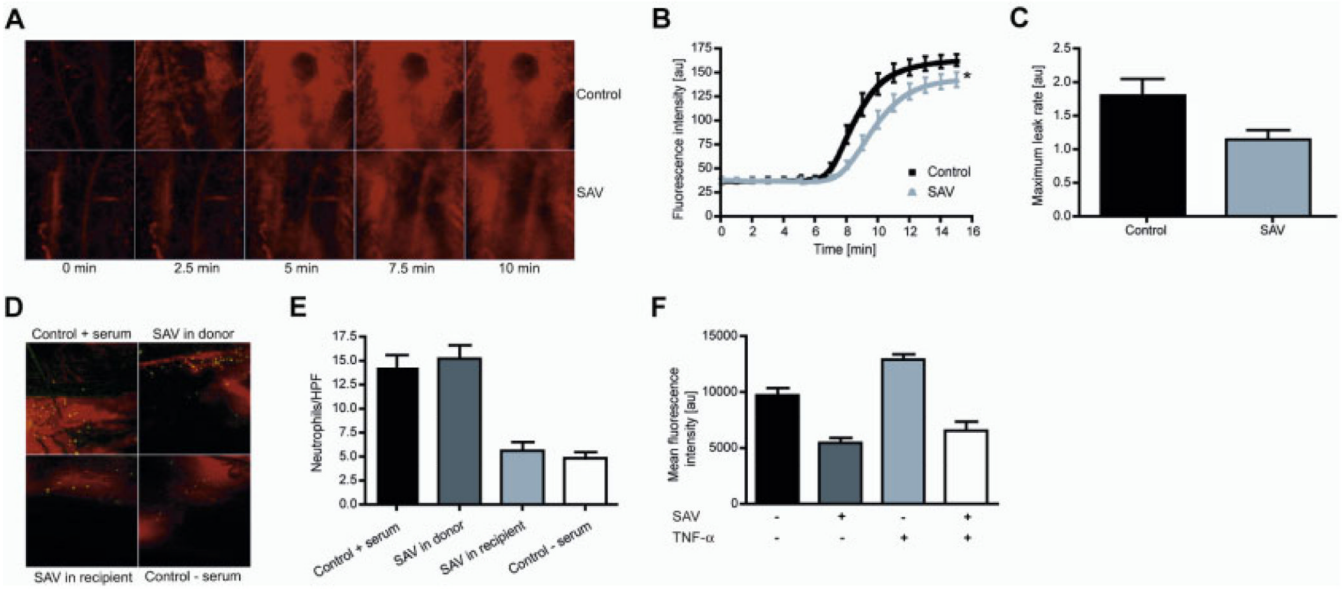

Figure 5.

Effects of self-activating viridin (SAV) treatment on endothelial cell functions. **A**, Representative images of early leakage after injection of K/BxN serum. A fluorescent vascular agent was injected before serum administration. Sequential images were taken for 10 minutes. **B**, Quantification of early leakage. There was a decrease in the maximum leakage rate and in the total leakage. Results are expressed as the mean fluorescence intensity (in arbitrary units [AU]). * = $P < 0.05$ versus controls. **C**, Quantification of the maximum leakage rate. The maximum leakage rate decreased by one-third. **D**, Representative images of neutrophil–endothelial interactions. Neutrophils (green) were isolated from donor mice, labeled in vitro, and injected into arthritic mice on day 6 of the disease course. SAV was given for 3 days prior to imaging. A vascular agent (red) was also injected to visualize vascular structures. **E**, Quantification of neutrophil–endothelial interactions. SAV treatment of donor neutrophils did not alter the attachment behavior of neutrophils, whereas administration of SAV to recipient mice reduced neutrophil attachment to baseline levels. Results are expressed as numbers of stationary neutrophils/high-power field (hpf). **F**, Flow cytometry of vascular cell adhesion molecule (VCAM) up-regulation in endothelial cells after treatment with tumor necrosis factor α (TNFα). SAV decreased the VCAM signal at baseline as well as after stimulation with TNFα. Values are the mean ± SEM of 6 mice per group in **B** and **C**, 3–4 mice per group in **E**, and 5 mice per group in **F**.

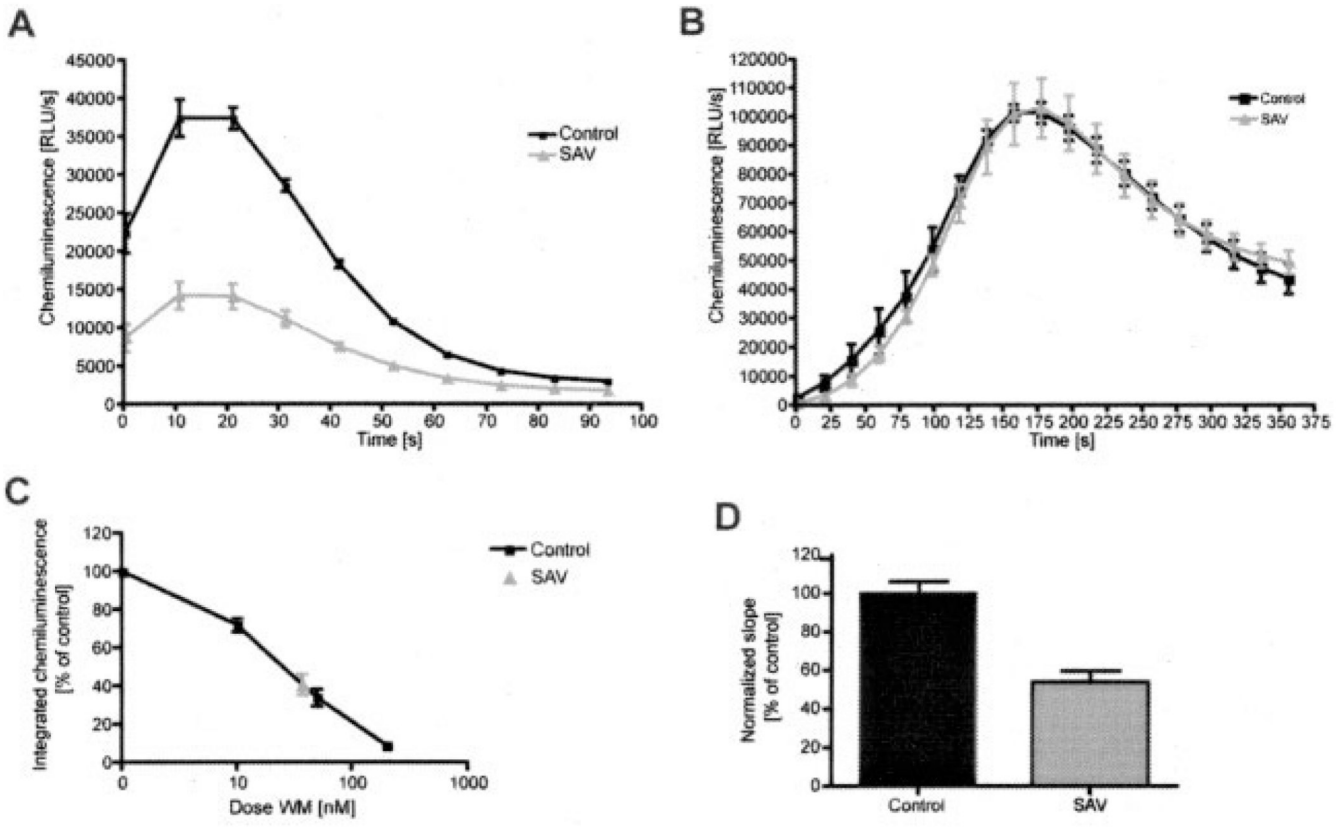

Figure 6.

Effects of self-activating viridin (SAV) treatment on neutrophil functions. **A**, Representative kinetics of oxidative burst after stimulation with formyl-Met-Leu-Phe (fMLP). Neutrophils from SAV-treated or control mice were exposed to fMLP as described in Materials and Methods. There was an apparent reduction in signal in SAV-treated neutrophils. Results are expressed in relative light units (RLU). **B**, Representative kinetics of oxidative burst after stimulation with phorbol myristate acetate (PMA). Neutrophils from SAV-treated or control mice were exposed to PMA as described in Materials and Methods. There was no difference between SAV-treated and control neutrophils. Values in **A** and **B** are the mean ± SEM of 3 mice (pooled). **C**, Bioactive concentration of wortmannin (WM) provided by SAV treatment. A dose-response curve generated using plain wortmannin was set in relation to the inhibition of oxidative burst with a 0.75 mg/kg concentration of SAV. The concentration of bioactive wortmannin is −41 n*M*. **D**, Quantification of fMLP-induced degranulation of proteolytic enzymes. SAV-treated and control neutrophils were analyzed for fMLP-induced degranulation of elastase in a colorimetric assay. SAV administration reduced degranulation by 47%. Values in **C** and **D** are the mean ± SEM of 3 experiments.